Intimations of K+ channel structure from a complete functional map of the molecular surface of charybdotoxin

ARTICLE *in* BIOCHEMISTRY · JANUARY 1994

Impact Factor: 3.02 · DOI: 10.1021/bi00168a008

3 AUTHORS, INCLUDING:

Christopher Miller
Brandeis University
97 PUBLICATIONS **3,068** CITATIONS

Intimations of K^+ Channel Structure from a Complete Functional Map of the Molecular Surface of Charybdotoxin†

Per Stampe,‡ Ludmilla Kolmakova-Partensky, and Christopher Miller*

Howard Hughes Medical Institute, Graduate Department of Biochemistry, Brandeis University, Waltham, Massachusetts 02254-9110

Received August 16, 1993®

ABSTRACT: The external vestibules of many K^+ channels carry a high-affinity receptor for charybdotoxin, a peptide of known structure. Point mutations of a recombinant toxin identified the residues directly involved in the interaction with a Ca^{2+}-activated K^+ channel. The interaction surface is formed from 8 of the 37 residues and covers about 25% of the peptide's molecular surface. The shape of the toxin permits a deduced picture of the complementary receptor site in the external vestibule of the K^+ channel.

Charybdotoxin (CTX) belongs to a class of peptide neurotoxins found in scorpion venoms (Miller et al., 1985; Gimenez-Gallego et al., 1988; Lucchesi et al., 1989). Acting in the 1 pM–10 nM concentration range, these toxins specifically block several types of K^+-selective ion channels, including many, but not all, voltage-gated and Ca^{2+}-activated K^+ channels (Miller et al., 1985; Gimenez-Gallego et al., 1988; MacKinnon & Miller, 1989; Wolff et al., 1988; Lewis & Cahalan, 1988). Channel block is produced by the binding of a single CTX molecule to a receptor site located in the outer "vestibule" of the channel, leading to the physical occlusion of the K^+ conduction pore (Anderson et al., 1988; Miller, 1988; MacKinnon & Miller, 1988).

Charybdotoxin is composed of 37 residues and contains three disulfide bonds. Its solution structure has been determined by NMR methods (Bontems et al., 1991, 1992), as has that of iberiotoxin, a CTX isoform (Johnson & Sugg, 1992). The toxin is a 20 × 20 × 25 Å globular structure formed by a three-turn α-helix lying upon a small three-strand antiparallel β-sheet. Mechanistic studies of channel block by CTX isoforms have revealed structural information about voltage-gated K^+ channels, including the gross locale of the conduction pore (MacKinnon & Miller, 1989; MacKinnon et al., 1990) and the tetrameric stoichiometry of the channel complex (MacKinnon, 1991). It is our intention here to exploit CTX as a finer structural probe of K^+ channels with which we may estimate physical dimensions near the external opening of the selectivity-determining K^+ conduction pore. As an early step in this effort, we now use specific mutagenesis of recombinant CTX (Park et al., 1991) in combination with mechanistic analysis of single Ca^{2+}-activated K^+ channels to map the functionally important parts of the toxin's molecular surface. The unusual shape of this interaction surface places strong constraints on the complementary surface of the external vestibule of the K^+ channel.

MATERIALS AND METHODS

Biochemical. Plasma membrane vesicles from rat skeletal muscle (Moczydlowski & Latorre, 1983) were used as the source of high-conductance Ca^{2+}-activated K^+ channels. Lipids used for planar bilayers were 1-palmitoyl-2-oleoylphosphaditylethanolamine (PE) and the corresponding phosphatidylcholine (PC), obtained from Avanti Polar Lipids, Inc. Charybdotoxin variants were produced by expressing a synthetic gene for a CTX-bearing fusion protein in *Escherichia coli*, as previously described (Park et al., 1991), with the following improvements in procedure. First, the factor Xa cleavage site (IEGR) was replaced with a site for enteropeptidase (DDDDK). Second, the medium used to dialyze the fusion protein was 10 mM Tris-HCl–1 mM 2-mercaptoethanol, pH 7.0. Third, CTX was released from the fusion protein by treatment with enteropeptidase ("enterokinase type 3B", Biozyme, Inc.), 100 units/mg of fusion protein at 37 °C for 24 h in dialysis medium containing 5 mM $CaCl_2$. All toxin mutants were well-behaved in both cation-exchange and reverse-phase HPLC purification steps (Park & Miller, 1992a) and gave final expression levels similar to wild-type toxin (50–100 nmol/L of culture).

Planar Bilayer Recording. Each toxin was assayed for activity by its kinetics of block of single Ca^{2+}-activated K^+ channels incorporated into planar lipid bilayers (PE, 14 mg/mL + PC, 6 mg/mL in *n*-decane), as described (Anderson et al., 1988). Experiments were performed in symmetrical 150 mM KCl solutions containing 10 mM Hepes, pH 7.4; open probability of each channel was maintained higher than 0.5 by adjusting the internal Ca^{2+} concentration in the range of 50–200 μM. After insertion of a single channel into the bilayer, further insertion was supressed by perfusion of the internal chamber with fresh solution, and a control record was collected for several minutes to establish stationarity of channel gating. Toxin was then added, with vigorous stirring, to the external solution, along with 30 μg/mL bovine serum albumin. The experimental record, containing 100–999 toxin blocking events, was stored on computer and videotape. Usually, records were taken at three voltages: 15, 30, and 45 mV. Most toxins were tested at three or more concentrations, to confirm the bimolecular nature of the blocking reaction.

Channel blocking data were analyzed in two different ways, according to the kinetics of toxin block. For slow toxins, with off-rates of less than 1 s^{-1}, an on-line pattern-recognition program was used to distinguish blocked intervals from unblocked intervals during which the channel fluctuates rapidly between open and closed states (Park & Miller, 1992a). For weak toxins, with off-rates in the range of 1–100 s^{-1}, statistical distributions of all open and shut dwell times were analyzed

† Supported by NIH Grant GM-31768 and Danish SNF Grants 11-7411 and 11-8644.

* To whom correspondence should be directed.

‡ Current address: Department of Physiology and Biophysics, University of Rochester Medical School, Rochester, NY.

® Abstract published in *Advance ACS Abstracts*, December 15, 1993.

0006-2960/94/0433-443$04.50/0

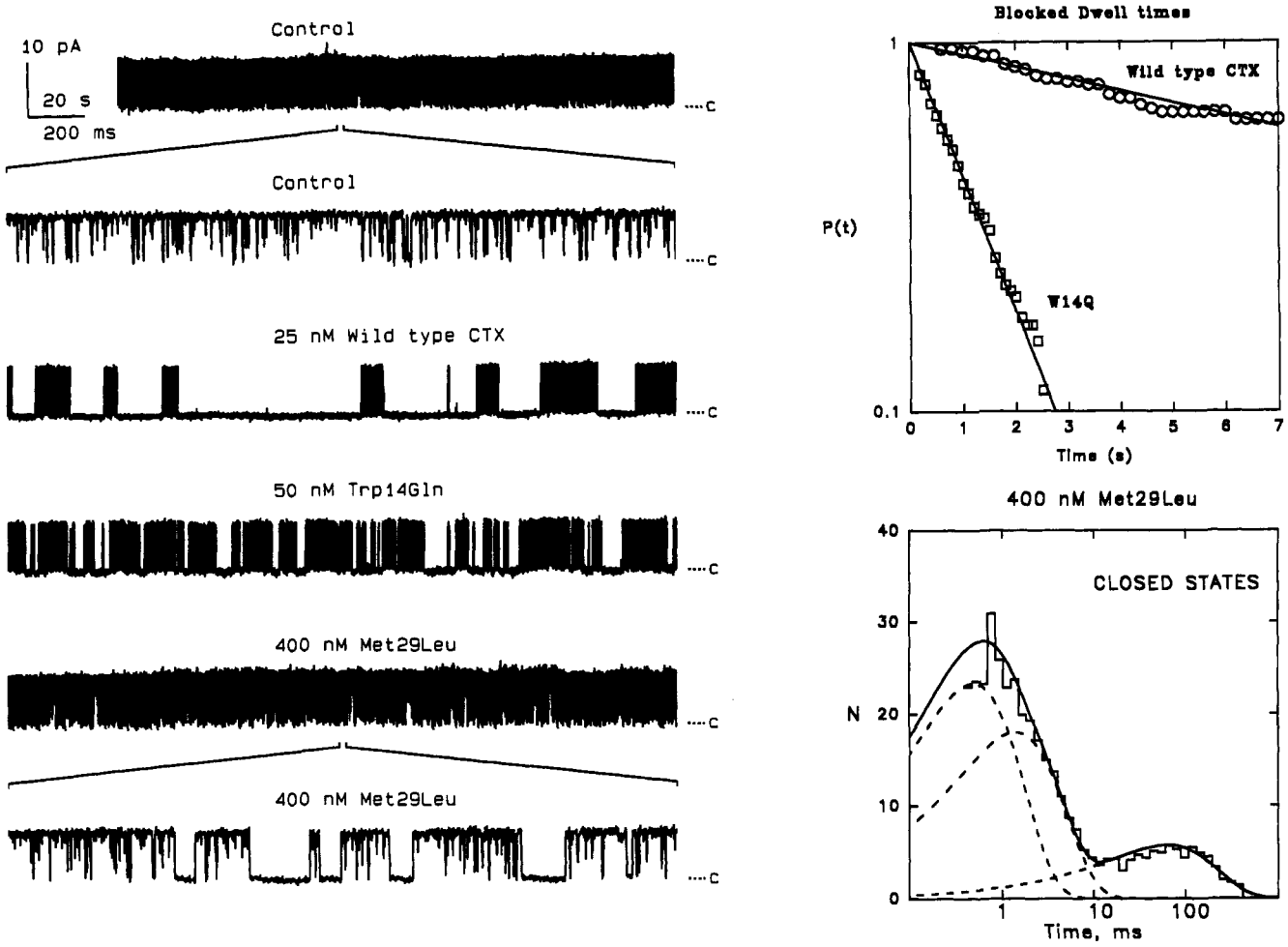

FIGURE 1: Single-channel assay of CTX mutants. The activity of each mutant CTX was assessed via the block of single high-conductance Ca^{2+}-activated K^+ channels from rat skeletal muscle plasma membranes incorporated into planar lipid bilayers. Channel openings are upward, and the closed state is marked on each trace. (A, left) Trace 1, control experiment with no CTX; trace 2, a portion of trace 1 with 100-fold expanded time base; trace 3, 25 nM wild-type CTX present; trace 4, 50 nM Trp14Gln; trace 5, 400 nM Met29Leu; trace 6, a portion of trace 5 with 100-fold expanded time base to reveal short-lived blocking events. (B, top right) Cumulative distribution of blocked events for wild-type CTX and Trp14Gln. $P(t)$ is defined as the probability that a blocked duration is greater than t. Lines are single-exponential fits with time constants of 16.2 s for wild-type CTX and 1.33 s for Trp14Gln. (C, bottom right) Full logarithmically binned histogram of 7500 nonconducting durations for Met29Leu showing three exponentials with time constants of 0.53, 1.51, and 69.3 ms. The longest closed state is absent in control experiments, and the amplitude increases linearly with toxin concentration (data not shown).

to isolate the population of toxin-induced blocked times. Rate constants for association and dissociation of toxin were calculated from the statistical distibutions of blocked and unblocked dwell times, as previously described (Anderson et al., 1988).

RESULTS

Previous work (Park & Miller, 1992a,b) focusing on the nine electrically charged residues of CTX showed that only three of these are functionally important and that they lie close together on the peptide's surface. We now determine the roles of the remaining residues that build this small, rigid peptide to see whether a well-defined interaction surface can be identified on the basis of functional alterations induced by single-residue replacements. We employ a minimal, high-resolution assay: the toxin's association–dissociation kinetics with single Ca^{2+}-activated K^+ channels incorporated into planar lipid bilayers. Figure 1 shows raw records of such experiments on wild-type CTX and two point mutants at strongly hydrophobic residues, W14Q and M29L. Each long-lived nonconducting interval represents a blocked state in which a single toxin molecule is bound to the single channel (Anderson et al., 1988).

From the statistical distributions of conducting and nonconducting dwell times, the association and dissociation rate constants for each toxin are readily derived (Anderson et al., 1988). Figure 1 illustrates raw data records and derived block-time distributions of channels exposed to either "slow" or "fast" toxins (see Materials and Methods). Each mutant discussed here behaves in a simple manner, showing a single population of blocked states (manifested in a single-exponential distribution of toxin-induced block times) and a pseudo-first-order association rate constant that varies linearly with toxin concentration.

Functional Effects of CTX Mutants. Because of its high disulfide content, CTX is a particularly good candidate for point mutagenesis work; the peptide is built on a rigid framework from which all non-cysteine side chains project into the solvent. It is unlikely, therefore, that a single point mutation will lead to gross misfolding of toxin. Nevertheless, for each toxin variant we were careful to examine independent criteria for correctness of toxin block (and by implication, structure) and locality of mutational alterations, such as voltage dependence in the presence of internal K^+, as described in detail (Park & Miller, 1992a,b). In several cases, we checked the backbone folding by 2-D NMR; two mutants

Table 1: Kinetics of K^+ Channel Block by Mutant CTX[a]

mutant	k_{off} ($\times 10^{-3}$ s^{-1})	k_{on} ($\times 10^6$ s^{-1} M^{-1})	K_D (nM)	n	mutant:WT k_{off}	mutant:WT k_{on}	mutant:WT K_D
WT	62 ± 3	7.0 ± 1.1	8.8	9	=1	=1	=1
F2A	350 ± 18	6.4 ± 1.7	55	4	5.6	0.91	6.3
F2W	510 ± 30	4.3 ± 0.6	120	8	8.3	0.61	13
T3S	98 ± 12	5.5 ± 0.3	18	6	1.6	0.78	2.0
T3L	380 ± 60	5.3 ± 0.3	71	7	6.1	0.76	8.1
N4D	74 ± 4	10.0 ± 1.5	7.4	8	1.2	1.4	0.84
V5E	100 ± 4	5.9 ± 0.8	17	5	1.6	0.84	1.9
S6D	64 ± 4	12.0 ± 1.8	5.3	6	1.0	1.7	0.6
T8S	30 ± 2	9.8 ± 0.9	3.1	5	0.48	1.4	0.35
T9V	59 ± 2	29 ± 4	2.0	4	0.95	4.1	0.23
S10T	220 ± 7	10.0 ± 1.6	22	5	3.5	1.4	2.5
S10A	910 ± 50	7.6 ± 0.7	120	7	15	1.1	14
S10Q	110 ± 10	0.0082 ± 0.0004	13000	3	1.8	0.0012	1500
W14F	770 ± 70	1.9 ± 0.1	410	8	12	0.27	47
W14Y	400 ± 16	1.1 ± 0.1	370	7	6.5	0.16	42
W14Q	750 ± 38	1.7 ± 0.2	430	7	12	0.24	48
W14M	1100 ± 80	1.6 ± 0.2	700	7	18	0.23	79
W14A	750 ± 110	2.3 ± 0.2	330	4	12	0.23	37
S15Y	100 ± 6	4.7 ± 0.7	22	6	1.6	0.67	2.5
V16E	110 ± 8	6.1 ± 1.2	18	4	1.7	0.87	2.0
Q18K	90 ± 7	8.5 ± 0.5	11	4	1.5	1.2	1.3
L20N	130 ± 9	4.7 ± 0.5	27	5	2.1	0.67	3.1
N22K	79 ± 5	7.3 ± 1.4	11	5	1.3	1.0	1.3
T23D	1900 ± 110	0.95 ± 0.07	2000	7	31	0.14	230
S24D	71 ± 5	5.1 ± 0.3	14	5	1.1	0.73	1.6
M29L	11000 ± 1000	6.6 ± 0.7	1600	6	180	0.94	180
M29I	53000 ± 6000	5.8 ± 0.3	9100	3	860	0.82	1000
M29K	11000 ± 200	0.73 ± 0.05	15000	4	180	0.10	1700
N30Q	3100 ± 400	15 ± 3	200	6	50	2.1	24
Y36F	72 ± 5	4.7 ± 0.3	15	5	1.2	0.67	1.7
Y36N	920 ± 220	3.5 ± 0.7	260	3	15	0.50	30
Y36L	56000 ± 2000	7.9 ± 0.9	7000	5	900	1.1	800
Y36A	91000 ± 3000	9.7 ± 1.5	9400	8	1500	1.3	1100
Y36H	89000 ± 1000	4.9 ± 0.5	19000	9	1400	0.70	2200
Y36P	120000 ± 3000	1.3 ± 0.1	94000	11	1900	0.19	11000
S37Q	140 ± 14	4.5 ± 1.4	30	5	2.3	0.64	3.4
S37X	740 ± 30	4.9 ± 0.4	150	7	12	0.70	17
T8S/T9G	210 ± 13	7.5 ± 0.8	28	5	3.4	1.1	3.2
T8S/T9V	26 ± 1	5.4 ± 0.2	4.8	3	0.42	0.77	0.55
R19Y/Y36F	79 ± 5	3.9 ± 0.8	20	6	1.3	0.44	2.3

[a] Association and dissociation rate constants of toxins, k_{on} and k_{off}, and the equilibrium dissociation constant, K_D, were measured at 30 mV on single Ca^{2+}-activated K^+ channels. Each value represents the mean ± SE of the number of measurements reported (n), each employing 100–1000 blocking events in a separate bilayer. The last three columns report values for the mutant toxins normalized to wild-type CTX. Values reported as dissociation rate ratios represent data previously published (Park & Miller, 1992a,b) and are as follows: Z1Q, 5.3; K11Q, 1.6; R19Q, 0.96; H21Q, 1.9; R25Q, 10.5; K27Q, 183; K27R, 3.4; K27N, 5.5; K27M, 820; K31Q, 2.8; K32Q, 0.93; R34Q, 8.8.

with strong effects on affinity, M29L and Y36A, showed spectra indicating a backbone structure identical to wild-type CTX (data not shown).

Table 1 summarizes the behavior of 53 CTX variants with mutations made at all 30 solvent-exposed positions. We left untouched the six cysteines and single glycine, which are strictly conserved among known CTX isotypes and together make up the toxin's buried interior. With only a few exceptions, we find that the altered affinities of mutant toxins are manifested primarily in perturbed dissociation rates, with little change in association rates, as expected for this diffusion-limited interaction (Miller, 1990).

These results allow us to classify most of the solvent-exposed residues of CTX as "crucial" or "indifferent" for channel-blocking function, as has been done for the charged residues (Park & Miller, 1992a). We define a residue as crucial if its replacement in a *chemically conservative manner* leads to an increase in off-rate of 8-fold or greater. Likewise, an indifferent residue is defined as one which, when subjected to a *chemically radical* change, affects the off-rate less than 3-fold. This distinction between the crucial and indifferent categories is, of course, arbitrary, but it falls naturally out of the results listed in Table 1. With these criteria, eight residues are classified as crucial for function: Ser10, Trp14, Arg25, Lys27, Met29, Asn30, Arg34, and Tyr36. Likewise, 16 residues fall into the indifferent category: Asn4, Val5, Ser6, Thr8, Lys11, Glu12, Ser15, Val16, Gln18, Arg19, Leu20, His21, Asn22, Ser24, Lys31, and Lys32. We also find four "equivocal" residues with off-rate increases between 3- and 6-fold for conservative alterations: pGlu1, Phe2, Thr3, and Ser37. The crucial residues include groups with a variety of chemical characteristics: positive charge (Lys27, Arg25, Arg34), strong hydrophobicity (Trp14, Met29, Tyr36), and H-bonding capacity (Ser10, Asn30). We imagine that the receptor site is reciprocally endowed with a varied chemical makeup and that specific block of toxin relies upon hydrophobic as well as polar interactions.

Two of the crucial hydrophobic residues, Trp14 and Tyr36, were investigated in some detail. Trp14 was replaced with Phe, Tyr, Asn, Met, and Ala. Remarkably, each of these mutants produces the same phenotype, an order of magnitude off-rate enhancement. These residues present widely different possibilities for chemical interactions but all are physically smaller than Trp. We suggest that Trp stabilizes toxin binding by about 1.5 kcal/mol via a favorable interaction, possibly with a hydrophobic group on the channel that cannot be

reached by the smaller residues on the toxin mutants. At position 36, Tyr was replaced with Phe, Asn, Leu, His, Ala, and Pro. Since Phe is a perfect substitute, the hydroxyl group on Tyr36 is unimportant for toxin binding. The small, polar Asn residue increases the off-rate 15-fold, so we may imagine that the Tyr makes a hydrophobic contact with the channel mouth. However, we cannot attribute the role of Tyr36 to hydrophobicity alone, since the Leu and Ala variants are about 3 orders of magnitude destabilized.

Nearly all these replacements yielded toxins with destabilized binding. However, replacing Thr8 by Ser actually stabilizes toxin binding with a 2-fold reduction in off-rate. This result is noteworthy because Ser occupies this position in iberiotoxin, a natural CTX isoform with a 13-fold lower off-rate than CTX, when assayed on this channel (Giangiacomo et al., 1992).

The small, polar residue Ser10 presents a unique anomaly. With Thr and Ala at this position, toxins follow the usual pattern, destabilization via an increased dissociation rate. But the Gln-substituted toxin, while giving a wild-type off-rate, displays a profoundly lowered (800-fold) association rate constant. (This is not an artifact due to misfolding of the mutant toxin, since this variant gives wild-type on-rate against the Shaker K^+ channel.) Thus, this point mutant creates an unusual kinetic barrier that must be overcome before the bound state can be reached.

The Toxin Interaction Surface. Figure 2 displays four views of the van der Waals surface of CTX, in which residues are color-coded according to the functional consequences of point mutations. The crucial residues are colored red, the indifferent ones green, and the equivocal residues yellow. The seven structurally untouchable residues are rendered in a connotatively neutral white, as are Thr9 and Thr23, which we cannot in good conscience dress in any of these colors as objectively defined.

A clear pattern emerges from these results: the 8 crucial residues are spatially separated from the 15 indifferent ones on the molecular surface of CTX. This conclusion was suggested in our previous survey (Park & Miller, 1992a) of the 9 charged residues and is now confirmed at higher spatial resolution. Of the 8 crucial residues, 6 project off the β-sheet toward the "bottom" of the molecule (downward in Figure 2 A,C). Arg25, Lys27, and Met29 project downward off the sheet's central strand (alternating with the buried residues Gly26 and Cys28); Asn30 begins a type I tight turn, which is followed by Arg34 and Tyr36 projecting downward from the third strand of the β-sheet (alternating with the buried, upward-pointing residues Cys33 and Cys35).

Viewed by a K^+ ion emerging from the channel's conduction pathway (Figure 2B), six of these residues form a flat triangular shape. To illustrate this, Figure 2E presents a schematic diagram of this view of the toxin, distinguishing the numbered red residues from the projected molecular boundary (dashed outline). The base of this triangle is formed by Arg25, Lys27, Met29, and Asn30, which lie vertically in this orientation in almost a straight line 20 Å long, while Tyr36 lies about 5 Å to the left of the center of the base. Arg34 lies on the line connecting Asn30 and Tyr36, slightly above the plane of the triangular core. The two remaining crucial residues, Ser10 and Trp14, define a line segment parallel to the core triangle's base located about 7 Å above the plane of this triangle and, in projection onto this plane, about 5 Å to the right.

The clean segregation of crucial from indifferent residues argues that the red surface depicted in Figure 2 is the area of intimate contact between toxin and channel. Henceforth, we explicitly assume this area to be the toxin's primary interaction surface. This conclusion is buttressed by various mechanistic characteristics of these mutations: the predominance of the off-rate in displaying sensitivity to mutation, the large energies involved in destabilizing toxins with chemically similar groups, and the known interaction of Lys27 with K^+ ions in the pore (Park & Miller, 1992b). A further indication of this picture is found in the location of the equivocal residues, which weakly but significantly affect dissociation kinetics. These yellow residues are all located adjacent to the interaction surface, on the side of the core triangle opposite to the edge of the red area defined by Trp14 and Ser10. The primary interaction surface has an area of roughly 850 $Å^2$, and the area covered by the yellow residues adds another 450 $Å^2$ to the region of toxin-channel contact. The 250-$Å^2$ exposed area of the white residues is small since these are mostly buried. The largest part of the toxin's molecular surface, the 1650-$Å^2$ green area, apparently makes no contact with the channel (Figure 2D) and is hence a good target for engineering of chemically reactive residues for future labeling studies.

DISCUSSION

A compelling reason to study CTX in such detail is the possibility of deducing structural features of the K^+ channel vestibule, the locale of the CTX receptor. To extrapolate from the form of the toxin's interaction surface to the shape of the channel is an uncertain endeavor requiring several explicit assumptions. We make these assumptions in a spirit of exploration, to discover how far the known structure of CTX may be mapped onto the unknown K^+ channel. First, we assume the complementarity principle: that a close steric fit between toxin and channel is essential for this specific, high-affinity interaction; this classical idea is well-supported in known cases of specific protein interactions with macromolecules, including antibody–antigen (Davies et al., 1990), protease–inhibitor (Huber et al., 1974), transcription factor–DNA (Schultz et al., 1991), enzyme–RNA (Rould et al., 1989), and, indeed, peptide–membrane receptor (deVos et al., 1992) pairs.

Second, we assume that the solution structure of CTX is not greatly perturbed by binding to the channel or by point mutation. For many small peptides, such an assumption would be wildly implausible, but for CTX it is tenable. The polypeptide backbone is rigidly constrained in its secondary structure by three disulfide bonds, and so it is unlikely that major rearrangements of this framework occur upon binding. Of course, we expect that small, localized changes of side-chain configurations will occur, as in the interaction of human growth hormone with its receptor (deVos et al., 1992); in that system, positions of side chains on the interaction surfaces are altered by less than 1 Å on average and by only 4 Å for the most extreme perturbation.

Third, we may safely assume that the Ca^{2+}-activated K^+ channel studied here, though of unknown sequence, is built along the lines of *Shaker*-type K^+ channels as a 4-fold symmetric tetramer of identical or similar subunits (MacKinnon, 1991; Christie et al., 1990; Liman et al., 1992). This assumption is justified by the functional similarity of this channel to the recently cloned *Slowpoke* Ca^{2+}-activated K^+ channel, which shows molecular similarity to voltage-gated K^+ channels (Atkinson et al., 1991; Adelman et al., 1992;

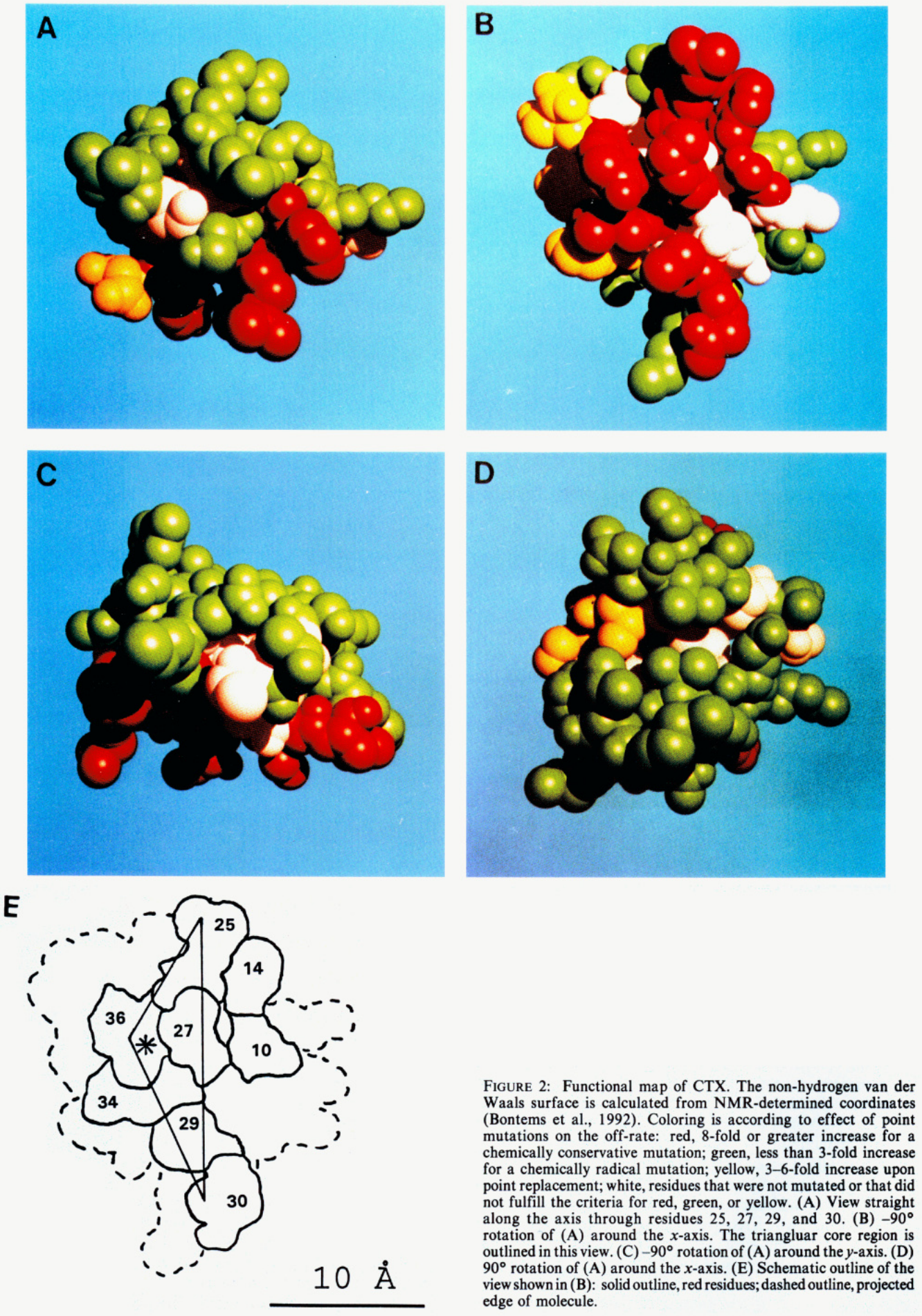

FIGURE 2: Functional map of CTX. The non-hydrogen van der Waals surface is calculated from NMR-determined coordinates (Bontems et al., 1992). Coloring is according to effect of point mutations on the off-rate: red, 8-fold or greater increase for a chemically conservative mutation; green, less than 3-fold increase for a chemically radical mutation; yellow, 3–6-fold increase upon point replacement; white, residues that were not mutated or that did not fulfill the criteria for red, green, or yellow. (A) View straight along the axis through residues 25, 27, 29, and 30. (B) –90° rotation of (A) around the *x*-axis. The triangluar core region is outlined in this view. (C) –90° rotation of (A) around the *y*-axis. (D) 90° rotation of (A) around the *x*-axis. (E) Schematic outline of the view shown in (B): solid outline, red residues; dashed outline, projected edge of molecule.

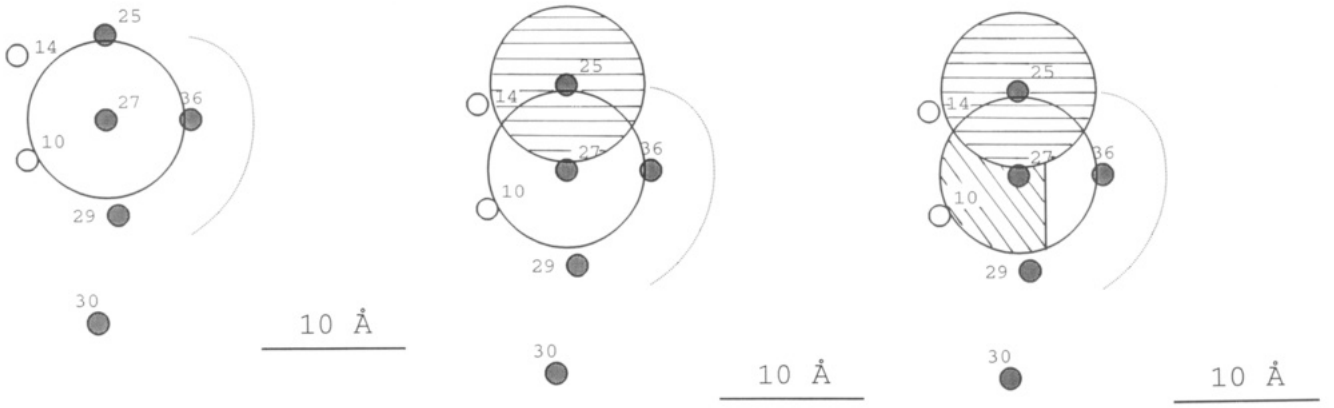

FIGURE 3: Placement of channel symmetry axis on CTX interaction surface. The positions of crucial residues, identified by numbers, are shown in the mirror-image view of Figure 2E. Filled dots identify residues on the bottom of the surface, while open dots represent residues in a plane 5–10 Å above this surface. The dashed curve shows the approximate edge of yellow residues. The striped area indicates regions forbidden for placement of the pore axis. (A, left) Axis must lie within 5 Å of Lys27. (B, center) Axis must lie farther than 5 Å of Arg 25. (C, right) Axis must be closer to yellow edge than to Ser10 and Trp14.

Butler et al., 1993). It has been shown (MacKinnon, 1991) that the homotetrameric *Shaker* channel displays four energetically equivalent CTX-binding sites, only one of which may be occupied at any time. Moreover, a homotetrameric mammalian *Slowpoke* channel incorporated into lipid bilayers shows CTX blocking kinetics identical to those seen here with the naturally expressed rat muscle plasma membrane channel (Naini & Miller, unpublished results).

Fourth, we demand that Lys27 is positioned physically close to a K^+ conduction site at the outer end of the narrow pore; this assumption arises from the known interaction between the ϵ-amino group of Lys27 and a K^+ ion occupying a site near the outer end of the conduction pathway (Park & Miller, 1992b). Accordingly, we place Lys27, which lies on the edge of the core triangle, within 5 Å of the channel's axis of symmetry. Moreover, the fact the Arg25 *fails* to interact with pore-associated K^+ (Park & Miller, 1992b) argues that this residue must be located farther away from the pore axis than is Lys27, i.e., greater than 5 Å. These are strong constraints which localize a small area on the toxin's interaction surface near the channel's axis of symmetry, i.e., near to a site for pore-associated K^+.

Using these four assumptions as a starting point, we ask what the CTX interaction surface may tell us about the channel. We suppose that the flat triangular core on the bottom of the toxin makes close contact with a complementary surface on the channel. On simple geometric grounds, the toxin's interaction surface must then span several subunits of the channel. It is impossible to position the toxin's elongated triangular core (Figure 2E) within a single projected 90° sector without simultaneously violating the constraints on the locations of Lys27 and Arg25. With the toxin's contact region spanning several identical subunits, equivalent positions on the symmetric receptor may contact *different* residues on the asymmetric toxin. There is ample precedent for such a situation (deVos et al., 1992), which leads in this case to a further deduction.

Specifically, we view the plane of the triangular core of the CTX interaction surface to be roughly normal to the channel's central axis. This conclusion relies on the 4-fold symmetry of the vestibule, which requires that the complementary shape matching the asymmetric toxin must be repeated four times. A significant pitch or yaw of the core triangle leads to shape inconsistencies in the receptor when repeated in 4-fold rotation. For example, since Arg25 and Met29 are about equidistant from Lys27 (near the center of symmetry), any 180° rotation will interchange the contact positions of these two residues; if the core triangle were tilted about a perpendicular from Tyr36, therefore, the receptor would have to display both a "hill" and a "valley" at the *same* position in projection. Examination of other pairs of contacts (such as Ser10 and Phe2) leads to similar inconsistencies unless the toxin's triangular core is placed normal to the channel's axis.

Finally, and most importantly, we attempt to position the toxin on the channel vestibule. In Figure 3, we illustrate the constraints placed on the location of the pore's axis of symmetry with respect to the CTX interaction surface. Here, we cartoon the interaction surface as a collection of dots representing each crucial residue, as seen from "above", i.e., viewed down through a transparent toxin bound to its receptor. Figure 3A displays the area within 5 Å of Lys27 within which the channel's symmetry axis must be located (assumption 4 above). However, part of this area (Figure 3B) is unavailble because it lies within 5 Å of Arg25.

An additional constraint arises from consideration of two other crucial residues, Ser10 and Trp14. These are located 5–10 Å above the bottom of the interaction surface and in projection about 5 Å off the triangular baseline. These elevated residues appear to make strong contact with a "wall" (or perhaps four "hills") at the outer edge of the vestibule. However, there are four yellow residues (dashed outline on Figure 3) located at the *same elevation* as Ser10 and Trp14 but on the opposite side of the toxin. A natural interpretation is that these yellow residues make weak contacts with positions on the receptor that are similar to those which Ser10 and Trp14 contact strongly on the opposite side of the vestibule. But this must mean that this yellow edge lies physically closer to the pore axis than do Ser10 and Trp14. This argument leads to a reduced area in which the pore axis is allowed (Figure 3C).

Taking into account, then, the constraints of shape consistency in 4-fold rotation and the key locations of Lys27 and Arg25, the channel's axis of symmetry should be located within a 2 × 2 Å area of the toxin interaction surface between Lys27 and Tyr36. The 4-fold rotation about this point creates an image (Figure 4A) mirroring the channel's interaction surface. Assuming strict complementarity, the receptor site forms a "plateau" of about 30 Å × 20 Å. This area defines a flat, pinwheel-shaped floor of the vestibule surrounding the opening of the narrow pore to the external solution. Because of the 4-fold symmetry of the receptor, there are four equivalent configurations in which a single toxin can bind (MacKinnon,

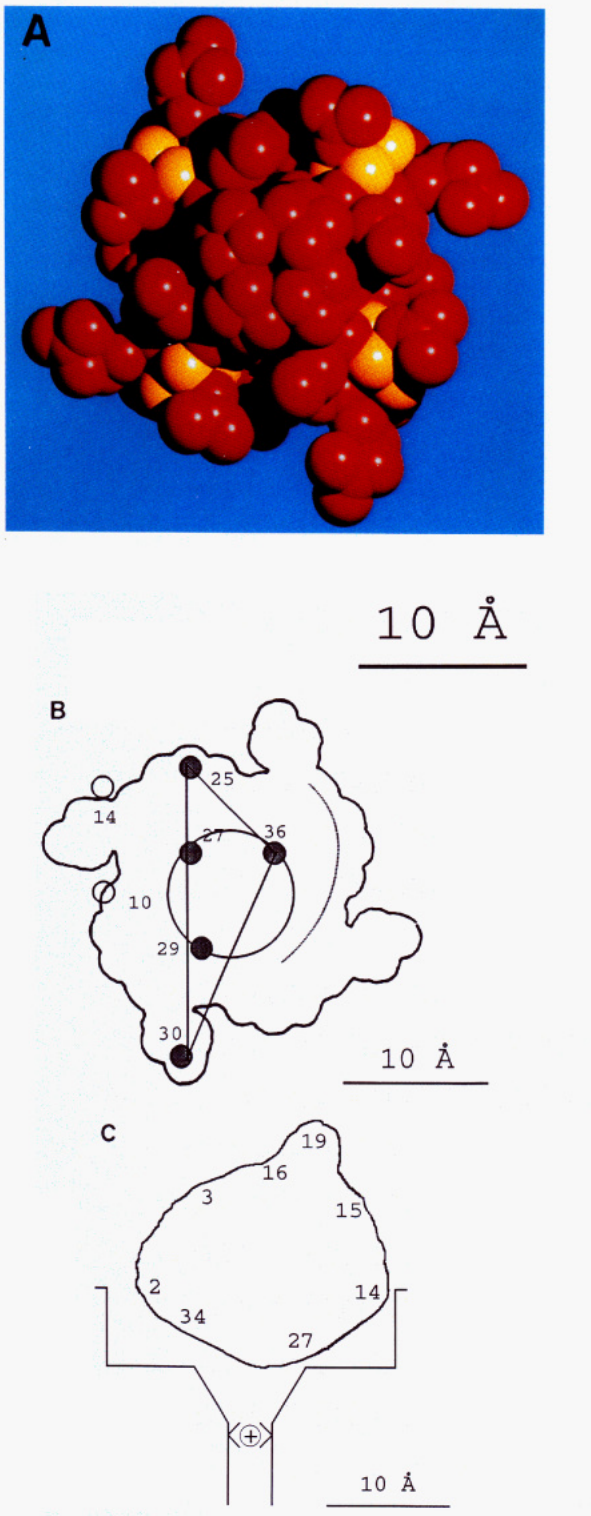

FIGURE 4: Charybdotoxin receptor. (A) The red and yellow part of the surface shown in Figure 2B is copied in 4-fold symmetry, creating a tetrameric interaction surface. In areas of overlap, the most protruding surface is shown in the display. The center of symmetry is placed between Lys27 and Tyr36, as outlined in the text. (B) Top view, looking downward through the CTX molecule, of the interaction surface residues positioned with respect to a 4-fold symmetric vestibule. (C) Hypothetical cross section through residues 14, 27, 34, and 2 and the center of the channel. Lys27, Arg34, and Trp14 are in close contact with the vestibule. Phe2 is positioned close enough to make weak contacts. Thr3, Ser15, Val16, and Arg19 are far away from any parts of the channel.

1991); Figure 4B gives an example of one such configuration.

The cartoon in Figure 4C presents a hypothetical cross section through the channel's axis of symmetry and through several key residues on the bound toxin. We picture a narrow (3-Å diameter) K^+-conduction pore widening abruptly at the CTX-binding plateau. A shallow 7-Å depression is drawn to accommodate the tetraethylammonium ion, which blocks this channel near to the CTX binding region (Miller, 1988; Giangiacomo et al., 1992). Moreover, the wall around the vestibule, defined by Ser10 and Trp14, cannot be much more than 10 Å high, since the green, noninteracting "top" of CTX overhangs the red residues. Of course, we cannot make any statements about the outside of the channel extending beyond the vestibule's 30-Å girth; however, K^+ channel transmembrane topology (Miller, 1991) suggests that only a small amount of the protein mass is exposed to the external solution.

We cannot emphasize strongly enough that our picture of the channel rests in its entirety upon a set of assumptions—shape complementarity to a rigid toxin, 4-fold channel symmetry, and the mechanistic behavior of toxin residues Lys27 and Arg25. None of these points has been proven with certainty, and each may be individually attacked on various grounds. Nevertheless, since all are strongly supported by a large body of experimental results, we have considered it worthwhile to embrace these assumptions as tentative "axioms" in order to see what structural features of the channel logically follow from them. The resulting picture is crude, but it is consistent with conventional expectations for the outer opening of an ion channel: a narrow ion-diffusion pore widening abruptly near the external solution (Miller, 1982; Toyoshima & Unwin, 1988). In order to accommodate the toxin's interaction surface, the vestibule pictured here must be quite flat and wide, on the order of 30 Å. The toxin blocks the channel by covering the outer opening of the narrow conduction pathway, while making multiple contacts with residues up to 15 Å distant from the center of the pore.

The surface map we have established for CTX sets the stage for using this molecule as a rigid molecular caliper for the outer regions of K^+ channels. We are currently extending this CTX-based approach to several genetically manipulable K^+ channels, in hopes of refining the method and estimating absolute distances between specific residues in K^+ channel vestibules.

ACKNOWLEDGMENT

We are grateful to J.-S. Hu for recording NMR spectra, to D. Peisach for molecular graphics, and to S. Goldstein and R. MacKinnon for advice throughout the course of this work.

REFERENCES

Adelman, J. P., Shen, K. Z., Kavanaugh, M. P., Warren, R. A., Wu, Y. N., Lagrutta, A., Bond, C. T., & North, R. A. (1992) *Neuron 9*, 209–216.

Anderson, C., MacKinnon, R., Smith, C., & Miller, C. (1988) *J. Gen. Physiol. 91*, 317–333.

Atkinson, N. S., Robertson, G. A., & Ganetzky, B. (1991) *Science 253*, 551–555.

Bontems, F., Roumestand, C., Boyot, P., Gilquin, B., Doljansky, Y., Menez, A., & Toma, F. (1991) *Eur. J. Biochem. 196*, 19–28.

Bontems, F., Gilquin, B., Roumestand, C., Menez, A., & Toma, F. (1992) *Biochemistry 31*, 7756–7764.

Butler, A., Tsunoda, S., McCobb, D. P., Wei, A., & Salkoff, L. (1993) *Science 261*, 221–224.

Christie, M. J., North, R. A., Osborne, P. B., Douglass, J., & Adelman, J. P. (1990) *Neuron 4*, 405–411.

Davies, D. R., et al. (1990) *Annu. Rev. Biochem. 59*, 439.

deVos, A. M., Ultsch, M., & Kossiakoff, A. A. (1992) *Science 255*, 306–312.

Giangiacomo, K. M., Garcia, M. L., & McManus, O. B. (1992) *Biochemistry 31*, 6719–6727.
Gimenez-Gallego, G., Navia, M. A., Reuben, J. P., Katz, G. M., Kaczorowski, G. J., & Garcia, M. L. (1988) *Proc. Natl. Acad. Sci. U.S.A. 85*, 3329–3333.
Huber, R., et al. (1974) *J. Mol. Biol. 89*, 73–101.
Johnson, B. A., & Sugg, E. E. (1992) *Biochemistry 31*, 8185–8159.
Lewis, R. S., & Cahalan, M. D. (1988) *Science 239*, 771–774.
Liman, E. R., Tytgat, J., & Hess, P. (1992) *Neuron 9*, 861–871.
Lucchesi, K., Ravindran, A., Young, H., & Moczydlowski, E. (1989) *J. Membr. Biol. 109*, 269–281.
MacKinnon, R. (1991) *Nature (London) 500*, 232–235.
MacKinnon, R., & Miller, C. (1988) *J. Gen. Physiol. 91*, 335–349.
MacKinnon, R., & Miller, C. (1989) *Science 245*, 1382–1385.
MacKinnon, R., Heginbotham, L., & Abramson, T. (1990) *Neuron 5*, 767–771.
Miller, C. (1982) *J. Gen. Physiol. 79*, 869–891.
Miller, C. (1988) *Neuron 1*, 1003–1006.
Miller, C. (1990) *Biochemistry 29*, 5320–5325.
Miller, C. (1991) *Science 252*, 1092–1096.
Miller, C., Moczydlowski, E., Latorre, R., & Phillips, M. (1985) *Nature (London) 313*, 316–318.
Moczydlowski, E., & Latorre, R. (1983) *Biochim. Biophys. Acta 732*, 412–420.
Park, C. S., & Miller, C. (1992a) *Biochemistry 31*, 7749–7755.
Park, C. S., & Miller, C. (1992b) *Neuron 9*, 307–313.
Park, C. S., Hausdorff, S. F., & Miller, C. (1991) *Proc. Natl. Acad. Sci. U.S.A. 88*, 2046–2050.
Rould, M. A., et al. (1989) *Science 246*, 1135–1142.
Schultz, S. C., et al. (1991) *Science 253*, 1001–1007.
Toyoshima, C., & Unwin, N. (1988) *Nature (London) 336*, 247–250.
Wolff, D., Cecchi, X., Spalvins, A., & Canessa, M. (1988) *J. Membr. Biol. 106*, 243–252.